Measuring Respiration and Heart Rate using Two Acceleration Sensors on a Fully Embedded Platform

Johan Vertens[1], Fabian Fischer[1], Christian Heyde[2], Fabian Hoeflinger[1], Rui Zhang[1], Leonhard Reindl[1] and Albert Gollhofer[2]

[1]*EMP, Albert-Ludwigs-University, Georges-Koehler-Allee 106, 79110 Freiburg, Germany*

[2]*Institut fuer Sport und Sportwissenschaft, Albert-Ludwigs-University, Schwarzwaldstraße 175, 79117 Freiburg, Germany*

Keywords: Respiration Rate, Heart Rate, Acceleration Sensor, Optimization, Bluetooth, Wearable Device.

Abstract: We present a novel system which measures the respiration rate using two three-axis accelerometers strapped to the chest and the back of a person. Respiration and heart rate are used as a measurement to determine an athlete's fitness level during the exercise phase. Common respiration rate measurement methods require devices which are mostly stationary or at least clunky and uncomfortable to wear for an extended period of time.

By using techniques such as differential measurement, pre-measurement optimization, adaptive filtering and peak detection we are able to obtain respiration rate even when the athlete is running fast. Our system is low-cost, small, and, by using a digital signal processor, fully capable of processing the data in an online way. Results are compared with a reference spirometer and have shown a very low normalized root mean square error (NRMSE) down to 1.42 %. Additionally, the heart rate of an athlete can be measured with the same sensor setup and similar methods.

1 INTRODUCTION

Ambulant and user friendly methods to derive an individual's physiological demand during rest and physical exercise are currently based on measurements of heart rate. However, heart rate mainly provides information about the cardiac loading rather than information about the metabolic strain - as for instance by certain stress thresholds derived from changes in the blood lactate concentration or the respiratory gas exchange (Wasserman, 2012). Thus, the accurate assessment of an individual's aerobic fitness level as well as the precise determination of an individual's intensity level for aerobic exercise are feasible only using a laboratory setting. The examination of the respiratory gas exchange usually requires clunky facemasks or mouthpieces which are uncomfortable to wear for an extended period of time to derive the needed measurements at the orifice.

Interestingly, there are some promising attempts demonstrating that simply the observation of changes in the respiration rate may facilitate stress threshold detection (Onorati et al., 2012; Carey et al., 2005). Deriving respiration rate during rest and exercise does not necessarily need the measurement at the orifice but can alternatively be derived from thoracic surface displacements (Heyde et al., 2014). Furthermore, the measurement of respiration rate solely needs the precise detection of the onsets of inspiration and expiration within a sinusoidal like data pattern. Therefore, it is hypothesized that common sensors that are surrounding the whole thorax (i.e. inductance plethysmographs) might be replaceable by smaller accelerometers which are able to register breathing induced thorax extension. In this pilot study, respiration rate values derived by means of an dual accelerometer system mounted at the chest and a gold standard flowmeter placed at the orifice were compared. Additionally, the system was used to simultaneously derive heart rate values in a similar way.

2 STATE OF THE ART

Currently, the respiration information can be measured by using many different sensor techniques. Our focus is to use inertial sensors for detecting the respiration rate. Inertial sensors are already used for different applications (Simon et al., 2015; Hoeflinger

Vertens, J., Fischer, F., Heyde, C., Hoeflinger, F., Zhang, R., Reindl, L. and Gollhofer, A..
Measuring Respiration and Heart Rate using Two Acceleration Sensors on a Fully Embedded Platform.
In *Proceedings of the 3rd International Congress on Sport Sciences Research and Technology Support (icSPORTS 2015)*, pages 15-23
ISBN: 978-989-758-159-5

et al., 2012a; Hoeflinger et al., 2011). In applications for human tracking they are already integrated into shoes or clothes (Hoeflinger et al., 2012b; Zhang et al., 2013) for detecting the body movement and measuring the path. Inertial sensors have been increasingly used in recent years to derive respiration rate. Accelerometers worn on the torso are capable of measuring inclination and angular changes during respiration. Afterwards, the respiration rate can be estimated using digital signal processing. Liu et al. present a method using adaptive band-pass filter and principal component analysis (PCA) to derive the respiratory rate from acceleration data (Liu et al., 2011). The method was capable of offering dynamic respiration rate estimation during various body activities such as sitting, walking, running, and sleeping. Tewel presents a new device for detection of apnoea, consisting of a three-axis MEMS accelerometer with digital output, microprocessor and some alarm instruments (Tewel, 2010). A wireless portable monitoring system to measure a user's respiratory airflow, blood oxygen saturation, and body posture is proposed in (Cao et al., 2012). The monitoring system consists of two sensor nodes including a hot-film flow sensor, triaxis accelerometer and oximeter. Phan et al. used an accelerometer to measure cardio-respiratory activity (Phan et al., 2008). The acquisition is realized in different modes: normal, apnoea, deep breathing or after exhaustion and also in different postures: vertical (sitting, standing) or horizontal (lying down). Yoon et al. suggest a method to improve the fusion of an accelerometer and a gyroscope by using a Kalman filter to produce a higher quality respiration signal (Yoon et al., 2014). The authors acclaim that the acceleration signal due to the movement can be easily removed because the frequency of movement acceleration is much higher than the frequency of respiration. However, it was found not true during our first attempt. Jin et al. proposed and analyzed three different methods to extract a single respiratory signal from the tri-axial data (Jin et al., 2009). The system is evaluated using simulated data from the most common postures, such as lying and sitting, as well as real data collected from five subjects. Bates et al. use a movement detection method to classify periods in which the patient is static and breathing signals can be observed accurately (Bates et al., 2010).

3 METHODS AND MATERIALS

3.1 Measurement Principle

With every breath a human takes his chest expands. We use two three-axis accelerometers centered at the front and the back of the torso of a person to measure the acceleration and inclination caused by the expansion of the chest. Both sensors are strapped to the torso with a flexible belt. Figure 1 shows the setup.

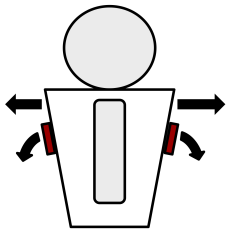

Figure 1: Setup of the two sensors (red). Translational and rotational directions are shown as arrows.

By using two sensors we can apply the method of differential measurement of the acceleration a, i.e. $a = a_{\text{front}} - a_{\text{back}}$. If a perfect alignment of the coordinate systems of both sensors is achieved, this method eliminates acceleration measurements introduced by translational movement which do not belong to the respiration.

After transformation and filtering of the data we detect the peaks of every amplitude and calculate the respiration and heart rate from the time difference between two adjacent peaks.

3.2 Hardware

For measuring and processing the acceleration data we designed two printed circuit boards which contain all the relevant digital blocks. The front pcb, which is mounted on the chest, contains the primary components as a STM32F4 microprocessor with an onboard DSP, a low energy bluetooth chip, a voltage regulator, flash memory and a LIS3DSH accelerometer. The back pcb holds the second LIS3DSH accelerometer and a port for connecting the two modules with each other. We have selected the sensors due to their very high sensitivities of 0.06 mg per bit in the measurement range ± 2.0 g with 16-bit data output. All communication between the digital parts is realized through SPI interface. Energy is delivered to the system via a small lithium battery. Communication to a PC or to a mobile device can be established via a serial or the bluetooth 4.0 connection. Since we have a very powerful setup we are able to perform all the signal processing onboard.

The size of the front pcb is 4.5 x 3.5 cm and contains also the mounting tabs for the chest strap while the back pcb is 2.3 x 2.0 cm. The hardware modules are shown in figure 2 and as a block diagram in figure 3.

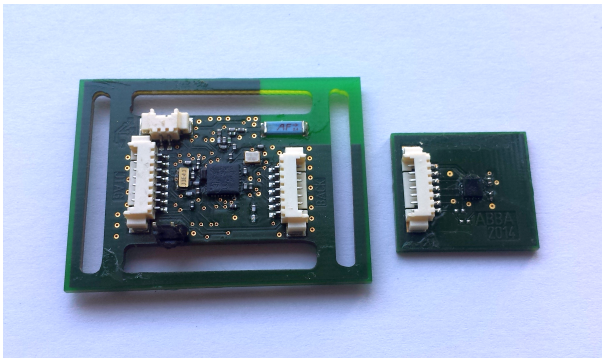

Figure 2: Hardware module for chest-mounting (left) and for back-mounting (right).

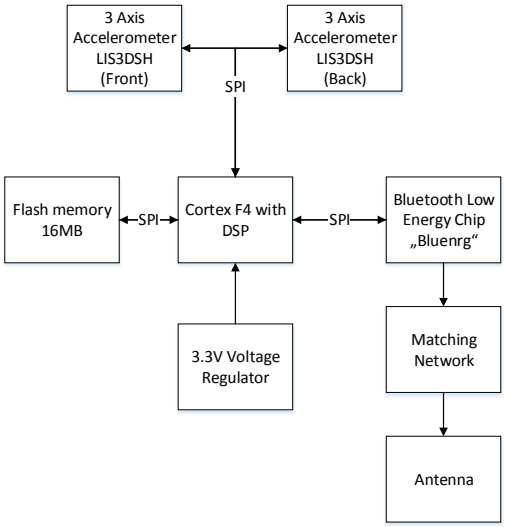

Figure 3: Block diagram of the hardware setup with the STM32F4 microprocessor, the two LIS3DSH accelerometers, the flash memory, the voltage regulator and the bluetooth chip with matching network and antenna. All communication between the digital parts is realized through SPI.

3.3 Calibration and Optimization

Slippage or unprecise mounting of the chest strap causes misalignment of the coordinate systems between the front sensor and the back sensor. Since we need perfect or at least very good alignment to generate the differential signal, we have developed a calibration routine for this purpose. In the case of misalignment, the differential measurement is not reliable any more. This is caused by accelerations which appear on different axes in the measurements of the two accelerometers.

At first the sensitivities and offsets of the sensors were calibrated following the least squares approach, whis is described in (STMicroelectronics, 2014). To align the two sensors we rotate the back sensor virtually until the coordinate systems are overlapping. For this procedure the rotation is described as rotation matrices for the x-, y- and z-axis with the corresponding angles Φ,Θ and Ψ. The coordinate system is visualized in figure 4.

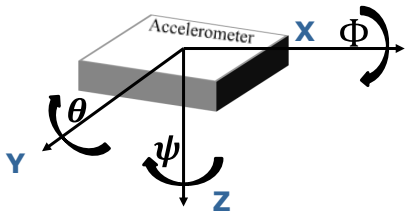

Figure 4: Coordinate system of an accelerometer.

$$R_x(\Phi) = \begin{bmatrix} 1 & 0 & 0 \\ 0 & \cos(\Phi) & -\sin(\Phi) \\ 0 & \sin(\Phi) & \cos(\Phi) \end{bmatrix} \quad (1)$$

$$R_y(\Theta) = \begin{bmatrix} \cos(\Theta) & 0 & \sin(\Theta) \\ 0 & 1 & 0 \\ -\sin(\Theta) & 0 & \cos(\Theta) \end{bmatrix} \quad (2)$$

$$R_z(\Psi) = \begin{bmatrix} \cos(\Psi) & -\sin(\Psi) & 0 \\ \sin(\Psi) & \cos(\Psi) & 0 \\ 0 & 0 & 1 \end{bmatrix} \quad (3)$$

The total rotation matrix for all three axis can then be formed by multiplying all matrices together:

$$A = R_x(\Phi^*) \cdot R_y(\Theta^*) \cdot R_z(\Psi^*) \quad (4)$$

Virtual rotation of the back sensor can be done by rotating the measurements x, y and z of the back accelerometer $S2$ with the rotation matrix A to the transformed measurements $\acute{x}$,$\acute{y}$ and $\acute{z}$:

$$\begin{bmatrix} \acute{x} \\ \acute{y} \\ \acute{z} \end{bmatrix}_{S2} = A \cdot \begin{bmatrix} x \\ y \\ z \end{bmatrix}_{S2} \quad (5)$$

If the rotation matrix is applied, the measurements of the front sensor $S1$ and the transformed measurements of the back sensor $S2$ are equal and the coordinate systems are overlapping:

$$\begin{bmatrix} \acute{x} \\ \acute{y} \\ \acute{z} \end{bmatrix}_{S2} = \begin{bmatrix} x \\ y \\ z \end{bmatrix}_{S1} \quad (6)$$

For a rough guess of the rotation matrix A we use the angular information which we directly get from the accelerometer measurements, namely the earth gravity vector. While standing still and holding the breath, there is no other acceleration affecting the measurement than the acceleration from gravity. In this situation the rotation angles Φ and Θ of the x- and y-axis for each sensor $S1$ and $S2$ can be determined with the following equations and the corresponding acceleration values a_x,a_y and a_z.

$$\Phi_{S1,S2} = tan^{-1}\left(\frac{a_y}{\sqrt{a_x^2+a_z^2}}\right) \tag{7}$$

$$\Theta_{S1,S2} = tan^{-1}\left(\frac{a_x}{\sqrt{a_y^2+a_z^2}}\right) \tag{8}$$

After calculating these angular guesses one can construct the angular differences Φ_d and Θ_d between the front and the back sensor by simple subtracting:

$$\begin{bmatrix}\Phi_d\\ \Theta_d\end{bmatrix} = \begin{bmatrix}\Phi_{S1}-\Phi_{S2}\\ \Theta_{S1}-\Theta_{S2}\end{bmatrix} \tag{9}$$

By using Φ_d and Θ_d in the corresponding equations 1 and 2 one can calculate the estimated rotation matrices, which transform the back sensor's coordinate system in order to fulfill equation 6. Since the wearer of the belt will probably do some motion in the calibrating phase which might distort the angle calculation and since the previously described method can only estimate the angles of the x- and y-axis, we further implemented a more advanced calibration, which takes the estimated angles, calculated from the earth gravity vector, as an initial guess.

3.3.1 Optimized Calculation of Rotation

In the more advanced approach for calculating the misalignment of the coordinate systems we introduce the cost function $C(\Phi,\Theta,\Psi)$ (equation 10) which calculates how good the fit between the measurements of the front sensor $S1$ and the back sensor $S2$ is.

$$\begin{aligned} C(\Phi,\Theta,\Psi) \quad = \quad & \frac{1}{N}\sum_{i}^{N}|x_i^{(S1)} - R_x(\Phi)x_i^{(S2)}| \\ & +|y_i^{(S1)} - R_y(\Theta)y_i^{(S2)}| \\ & +|z_i^{(S1)} - R_z(\Psi)z_i^{(S2)}| \end{aligned} \tag{10}$$

After collecting data for some seconds the cost function can be optimized over the rotation angles Φ,Θ and Ψ (equation 11), in order to get the optimized angles Φ^*,Θ^* and Ψ^*. For getting useful data one must still hold the breath in the collecting phase since we just want information which is about static positioning on the body. Dynamic movement along an axis of the body while collecting measurement data helps the optimizer to calculate a good result in contrast to the previous estimation approach, presented in chapter 3.3, where no movement should occur.

$$\begin{bmatrix}\Phi^*\\ \Theta^*\\ \Psi^*\end{bmatrix} = \arg\min_{\Phi,\Theta,\Psi} C(\Phi,\Theta,\Psi) \tag{11}$$

Since the processing speed of a microcontroller is limited we used the stable and easy to implement local search optimizer for solving equation 11. The calculated angles from the previous method from chapter 3.3 can be fed into the optimizer as an initial guess, which leads to faster convergence. Figure 5 shows the result of the optimization of a sample data set. The data set was generated by random acceleration of a slightly misaligned sensor setup.
The whole alignment procedure is done only once during startup of the system. Afterwards the rotation matrix is stored internally and applied to every new measurement.

3.4 Adaptive Filter

To eliminate noise outside of the respiration rate spectrum, we use an IIR Butterworth bandpass filter on the acceleration data. The cutoff frequencies for respiration rate filtering were set to F_{low} = 0.1 Hz and F_{high} = 0.8 Hz. With only this bandpass the noise in our signal is still too large. Therefore we implemented an adaptive filter which works in the following way:

- At first the data is filtered through a wide 4 stage IIR Butterworth bandpass with 0.1 Hz to 0.8 Hz.
- Then a spectrum over the last 1 minute of filtered data is calculated using a FFT. When the intention is to analyze respiration with higher variance this time frame can be made shorter.
- The maximum power frequency f_{max}, which is extracted from the FFT, is used to build a new narrow 4 stage IIR bandpass with bandwidth f_{bw}. The high border is then calculated as $f_h = f_{max} + f_{bw}$ while the lower border is calculated with $f_l = f_{max} - f_{bw}$. For still activities we chose $f_{bw} = 0.25\ Hz$ and for sport activities $f_{bw} = 0.50\ Hz$. The widths of the bandpasses are chosen in a way that the high variance of the respiration frequency while doing sport is taken into consideration. In situations with less activity like sitting or sleeping it can be expected that the variance of the respiration rate is reasonable lower. The corresponding IIR coefficients are stored in a

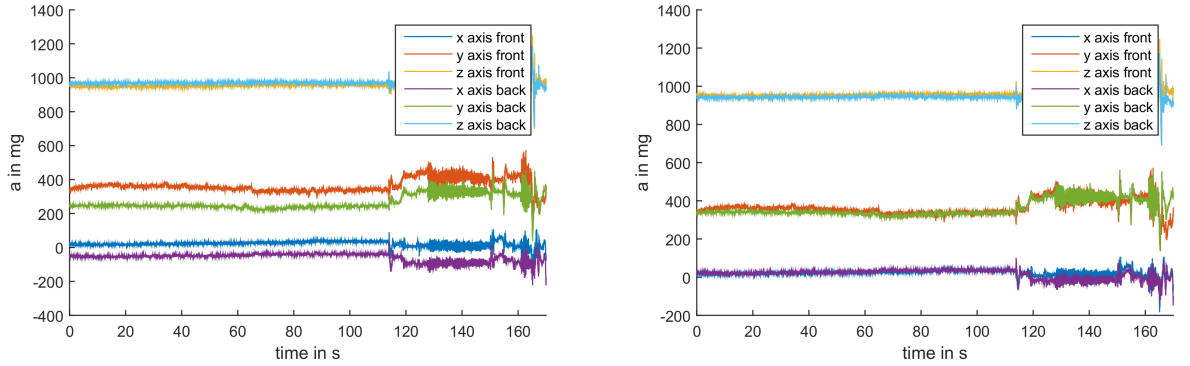

Figure 5: Left side: Not optimized acceleration data. Here the coordinate systems are misaligned. Right side: Optimized acceleration data. The coordinate systems are overlapping.

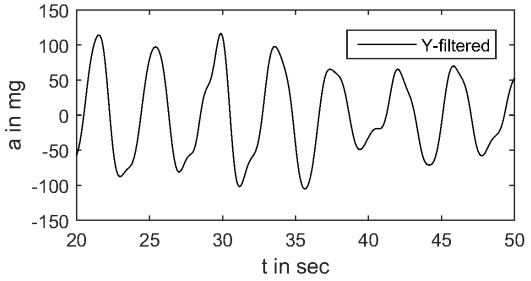

Figure 6: Filtered difference acceleration signal a_{diff}.

database on the chip and the coefficients which fit best to the calculated frequency band f_h to f_l are then applied.

3.5 Peak Detection

After optimization, rotation and filtering we solely use the y-axis acceleration data a_y, which is in the direction normal to the chest and the back surface. This is the part of the data with the highest information value to detect the lifting and inclination of the chest at respiration.

The final difference acceleration data a_{diff} is then calculated by subtracting the back sensor data $a_{y_{\text{back}}}$ from the front sensor data $a_{y_{\text{front}}}$. This reduces the errors introduced by motion of the subject. The resulting data is represented in figure 6.

We then use an embedded peak detection algorithm to detect maxima in the data. The algorithm stores the last 18 seconds of the data in a buffer and checks for peaks by looking at every data point A_i. If the leftmost neighbor A_{i-1} and rightmost neighbor A_{i+1} are smaller than A_i, i.e. $A_{i-1} \leq A_i \leq A_{i+1}$, A_i is a peak candidate. The algorithm then calculates the peak prominence p_i of A_i. The peak prominence is defined as vertical height between the peak and the nearest minimum belonging to a higher peak. If there is no higher peak it is defined as vertical height between the peak and the lowest data point.
If the peak candidate A_i has an equal or higher peak prominence p_i than 0.5 times the standard deviation σ of the data in the buffer, i.e. $p_i \geq 0.5 \cdot \sigma$, it is stored as a true peak P_i.
After one second the buffer is shifted by 100 points, the new 100 data points are stored and the search for a new peak is repeated. This means the possible update frequency for respiration rate output of our system is 1 Hz.

3.6 Respiration Rate Calculation

From the position of two peaks in the buffer of the peak detection method introduced in section 3.5 and sampling rate F_s = 100 Hz, we can calculate the time T_d between two peaks as can be seen in equation 12. The resulting respiration rate F_R is the inverse of T_d, i.e. $F_R = \frac{1}{T_d}$.

$$T_d = \frac{|P_i - P_j|}{F_s} \tag{12}$$

3.7 Heart Rate Detection

For parallel heartbeat detection we use the aligned differential acceleration signal with a higher sampling rate of 400 Hz. In the unfiltered signal of the y-axis the pulses are already clearly visible (see figure 7). Unfortunately this signal is not very suitable for direct extraction of the heartbeat.
It turns out that for our measurement system the heartbeat pulses appear as blocks of several swings with the frequency between 12 and 28 Hz. For filtering out the undesired noise we then filter the signal with a 12-28 Hz IIR Butterworth bandpass filter. Afterwards we take the absolute value of the IIR filtered signal (see figure 8).
Finally we smooth the signal with a second order FIR savitzky golay filter and window of 49 samples, which

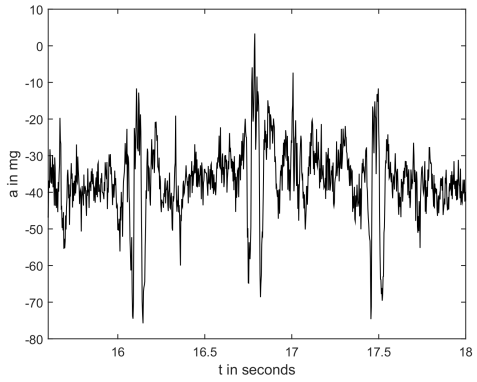

Figure 7: Raw heartbeat signal from differential signal.

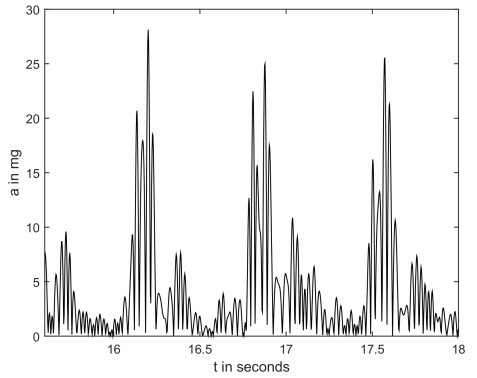

Figure 8: IIR filtered absolute heartbeat signal.

keeps the relative maxima, minima and diversification (see figure 9). Over the resulting signal we use again our embedded peak detector to obtain the heart rate.
For filtering out outliers, we compare the mean of the last 5 valid frequencies with the new calculated frequency. If the new one is more than 50% away from the previous mean it is discarded. At initialization of the device, when there are no previous frequencies, we just take the mean of the first 10 frequencies as the value for comparison. Only after the initialization the heartbeat frequency will be outputted.

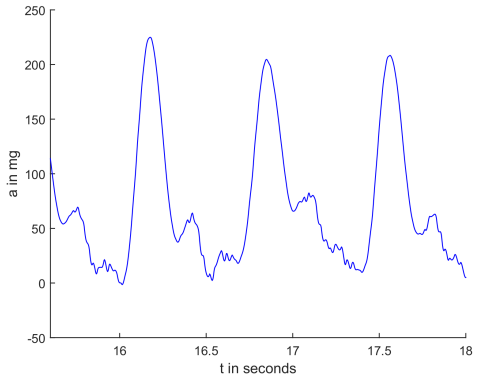

Figure 9: Savitzky golay filtered heartbeat signal.

4 RESULTS

To verify our system we performed several test measurements. Two subjects A and B, outfitted with our system, were standing, walking and running on a treadmill. The reference respiration rate was derived from a stationary CPX system (Oxycon Pro Care Fusion, San Diego CA, USA). Optoelectronic flow detection occurred by a flow-volume sensing turbine inside a transducer holder fixed on the subjects facemask. Prior to testing, the flow-volume sensing turbine was calibrated by a 3 liter syringe. Figure 10 shows the experimental setup.

Figure 10: Experimental setup for evaluation of the system with subject A (left) and B (right).

To smooth the resulting frequencies we applied a 10 second moving average filter to the measurement and reference data. The first minute of data was skipped due to calibration and optimization issues.
The error between the measurement and the reference is stated both as normalized root mean square error (NRMSE) and mean percentage error (MPE). The calculation of the NRMSE is done as shown in equation 13, where the measurement range is from $F_{\min}$ = 0.1 Hz to $F_{\max}$ = 0.8 Hz for respiration rate measurements and from $F_{\min}$ = 0.8 Hz to $F_{\max}$ = 3.5 Hz for heart rate measurements. The MPE is calculated according to the equation 14. All data presented here are recorded from subject A, since the T-shirt worn by subject B influenced the measurements and made them unreliable.

$$E_{\text{NRMSE}} = \frac{\sqrt{\frac{\sum_{i=1}^{N}(F_{\text{meas}_i} - F_{\text{ref}_i})^2}{N}}}{F_{\max} - F_{\min}} \tag{13}$$

$$E_{\text{MPE}} = \frac{\sum_{i=1}^{N} \frac{\left|F_{\text{meas}_i} - F_{\text{ref}_i}\right|}{F_{\text{ref}_i}}}{N} \tag{14}$$

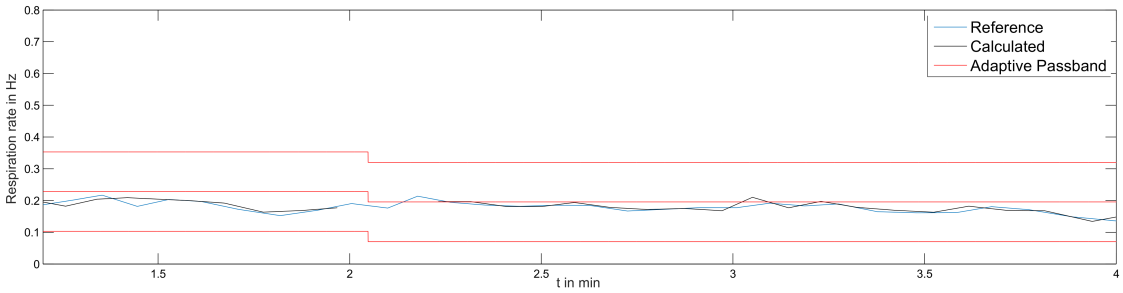

Figure 11: Respiration rate measurement of our system (black) and the reference (blue) in situation S1. The borders of the adaptive bandpass are marked in red.

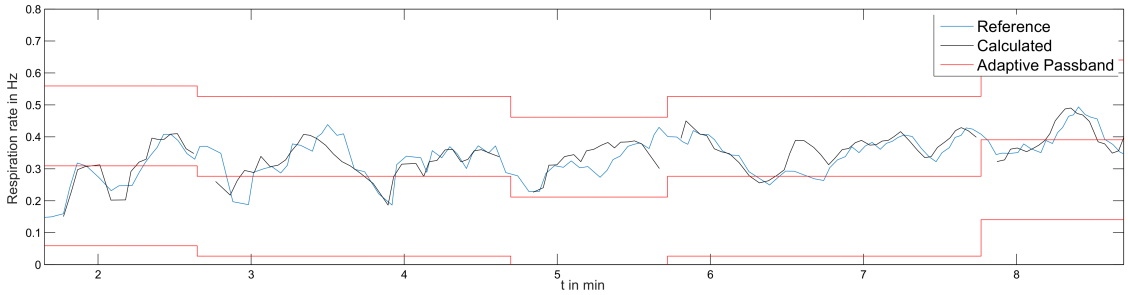

Figure 12: Respiration rate measurement of our system (black) and the reference (blue) in situation S2. The borders of the adaptive bandpass are marked in red.

4.1 Respiration Rate

To quantify the performance of our system in distinct use cases we reconstructed three different situations.

Situation One (S1): Office work.
The subject was sitting on an office chair, performing slight motion which involved moving the upper body and the arms. The measurement time was 4 minutes. Figure 11 shows the respiration rate of our system and the reference.

Situation Two (S2): Walking and jogging.
The subject was first walking with 5 $\frac{\text{km}}{\text{h}}$ for 5 minutes, then jogging with 7 $\frac{\text{km}}{\text{h}}$ for 4 minutes on a treadmill. The measurements can be seen in figure 12.

Situation Three (S3): Running and stopping.
The subject was running with 15 $\frac{\text{km}}{\text{h}}$ on a treadmill followed by 2 minutes of standing still. This was then repeated, as can be seen in figure 13.

Table 1 shows the NRMSE and MPE of our system measurements compared to the reference in the three situations.

Table 1: NRMSE and MPE of respiration rate measurement.

Situation	NRMSE	MPE
S1	1.42 %	4.40 %
S2	5.46 %	8.59 %
S3	3.95 %	4.13 %

4.2 Heart Rate

To quantify the performance of or system at measuring the heart rate we used a Polar H7 heart rate belt strapped to the chest of the subject as the reference. For this test the situation was slight movement of the subject, which included body rotation and walking across a room for 4 minutes. The heart rate measurement of our system and the reference measurements can be seen in figure 14. The NRMSE and PME are stated in table 2.

Table 2: NRMSE and MPE of heart rate measurement.

	Situation: Slight movement
NRMSE	1,74 %
MPE	2,65 %

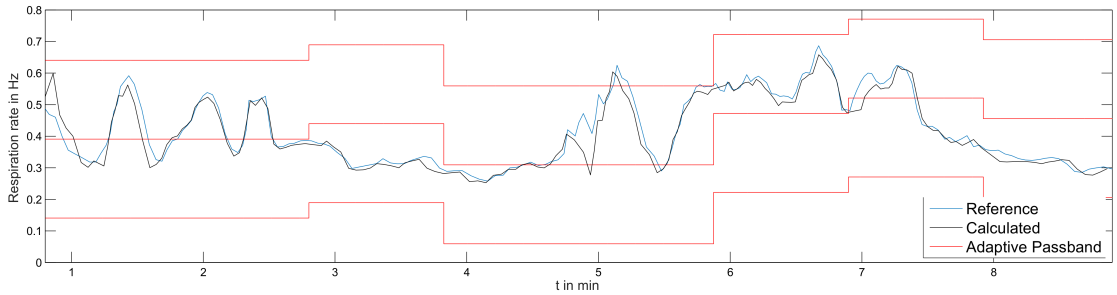

Figure 13: Respiration rate measurement of our system (black) and the reference (blue) in situation S3. The borders of the adaptive bandpass are marked in red.

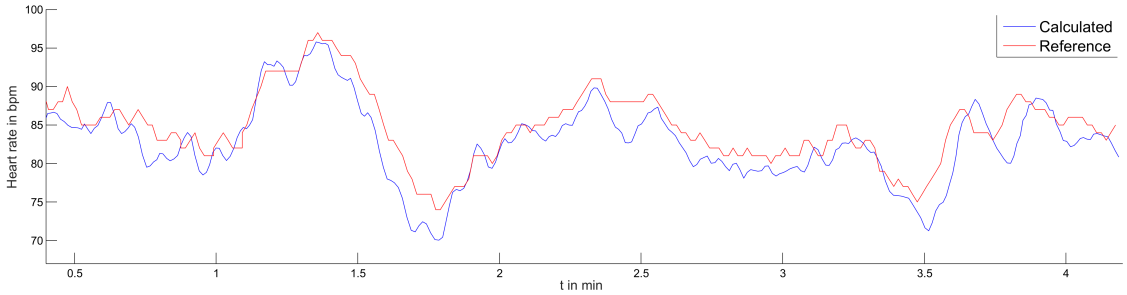

Figure 14: Heart rate measurement of our system (blue) and the reference (red).

5 CONCLUSIONS

In this paper, a method to measure respiration and heart rate with acceleration sensors has been presented. The results show that we are able to detect the respiration rate with low errors in different situations. By using the differential measurement with two sensors, advanced calibration, optimization methods, and an adaptive, rather small bandpass, we are able to reduce the noise drastically and receive reliable results, even in very noisy settings such as fast running.

Important to recognize is, that the highest error occurs if the person has a medium activity like in situation S2. In this situation the signal-to-noise ratio is very weak due to the relatively small demand of oxygen and the corresponding small amplitude of the chest. Surprisingly the ratio increases again with a more demanding activity and higher amplitude of the chest, although this activity results in a higher motion noise, like in situation S3. This observation explains the fact that smaller errors can be achieved in very still activities as well as in intensive sport activities. In these situations our dual sensor setup produces highly accurate measurements, while the results in situation S2 are still very reasonable.

Since it occurred to us that most of the information came from the inclination of the sensor during respiration, further investigations could be done with gyroscopes in comparison to acceleration sensors.

Furthermore, by using the same sensor setup and similar methods we were able to measure the heart rate with a very small error. Further development of the heart rate detection component and an application of our methods to more different situations could be a promising topic for future investigations.

REFERENCES

Bates, A., Ling, M., Mann, J., and Arvind, D. (2010). Respiratory rate and flow waveform estimation from tri-axial accelerometer data. In *Body Sensor Networks (BSN), 2010 International Conference on*, pages 144–150.

Cao, Z., Zhu, R., and Que, R.-Y. (2012). A wireless portable system with microsensors for monitoring respiratory diseases. In *Biomedical Engineering, IEEE Transactions on*, volume 59, pages 3110–3116.

Carey, D. G., Schwarz, L. A., Pliego, G. J., and Raymond, R. L. (2005). Respiratory Rate is a Valid and Reliable Marker for the Anaerobic Threshold: Implications for Measuring Change in Fitness. volume 4, pages 482–488.

Heyde, C., Leutheuser, H., Eskofier, B., Roecker, K., and Gollhofer, A. (2014). Respiratory inductance plethysmography-a rationale for validity during exercise. volume 46, pages 488–495.

Hoeflinger, F., Mueller, J., Toerk, M., Reindl, L., and Burgard, W. (2012a). A wireless micro inertial measure-

ment unit (IMU). In *Instrumentation and Measurement Technology Conference (I2MTC), 2012 IEEE International*, pages 2578–2583.

Hoeflinger, F., Toerk, M., Ojha, A., and Reindl, L. (2011). Drivability enhancement of transport buses using an auxiliary system with an IMU. *International Journal of Electrical & Computer Sciences (IJECS)*.

Hoeflinger, F., Zhang, R., and Reindl, L. (2012b). Indoor-localization system using a micro-inertial measurement unit (IMU). In *European Frequency and Time Forum (EFTF), 2012*, pages 443–447.

Jin, A., Yin, B., Morren, G., Duric, H., and Aarts, R. (2009). Performance evaluation of a tri-axial accelerometry-based respiration monitoring for ambient assisted living. In *Engineering in Medicine and Biology Society, 2009. EMBC 2009. Annual International Conference of the IEEE*, pages 5677–5680.

Liu, G. Z., Guo, Y. W., Zhu, Q. S., Huang, B. Y., and Wang, L. (2011). Estimation of respiration rate from three-dimensional acceleration data based on body sensor network. In *Telemed J E Health*, volume 17, pages 705–711.

Onorati, P., Martolini, D., Valli, G., Laveneziana, P., Marinelli, P., Angelici, E., and Palange, P. (2012). A simplified approach for the estimation of the ventilatory compensation point. volume 44, pages 716–724.

Phan, D., Bonnet, S., Guillemaud, R., Castelli, E., and Pham Thi, N. (2008). Estimation of respiratory waveform and heart rate using an accelerometer. In *Engineering in Medicine and Biology Society, 2008. EMBS 2008. 30th Annual International Conference of the IEEE*, pages 4916–4919.

Simon, N., Bordoy, J., Hoeflinger, F., Wendeberg, J., Schink, M., Tannhaeuser, R., Reindl, L., and Schindelhauer, C. (2015). Indoor localization system for emergency responders with ultra low-power radio landmarks. In *International Instrumentation and Measurement Technology Conference (I2MTC)*.

STMicroelectronics (2014). AN4508 Application note - Parameters and calibration of a low-g 3-axis accelerometer.

Tewel, N. (2010). Application of mems accelerometer for baby apnea monitoring under home conditions. In *Acta Bio-Optica et Informatica Medica. Inynieria Biomedyczna*, volume Vol. 16, nr 4, pages 389–393.

Wasserman, K. (2012). *Principles of exercise testing and interpretation: Including pathophysiology and clinical applications*. Wolters Kluwer/Lippincott Williams & Wilkins, Philadelphia, 5th edition.

Yoon, J., Noh, Y., Kwon, Y., Kim, W., and Yoon, H. (2014). Improvement of dynamic respiration monitoring through sensor fusion of accelerometer and gyro-sensor. *Journal of Electrical Engineering and Technology*, 1(1).

Zhang, R., Bannoura, A., Hoeflinger, F., Reindl, L., and Schindelhauer, C. (2013). Indoor localization using a smart phone. In *Sensors Applications Symposium (SAS), 2013 IEEE*, pages 38–42.